Atom cooling by partially spatially coherent lasers

Jing-Fang Zhang, Zhao-Ying Wang,* Bing Cheng, Qi-Yu Wang, Bin Wu, Xiao-Xia Shen, Li-Ling Zheng, Yun-Fei Xu, and Qiang Lin†

Institute of Optics, Department of Physics, Zhejiang University, Hangzhou 310027, China

(Received 29 November 2012; revised manuscript received 31 January 2013; published 16 August 2013)

Atom cooling and trapping by partially spatially coherent lasers is investigated both experimentally and theoretically. The degree of spatial coherence of the laser beams is controlled by the electro-optic crystal. The characteristics of the trapped atomic cloud are studied. The experimental results indicate that the atom number and atomic Gaussian density distribution stay unchanged due to the fact that the average photon scattering rate is independent of the spatial coherence of the laser beams. However, the measured temperature of the atomic cloud increases as the degree of spatial coherence of the laser beams decreases. The reason is that the scattering force of the partially spatially coherent lasers acting on the atoms fluctuates temporally and spatially, which broadens the velocity distribution of the atoms.

DOI: 10.1103/PhysRevA.88.023416 PACS number(s): 37.10.De, 42.25.Kb, 42.50.Ct

I. INTRODUCTION

The laser beams used in atom cooling and trapping are generally regarded as coherent both temporally and spatially. However, some experiments show that atoms can also be cooled efficiently by isotropic diffuse light [1–3]. The diffuse light cooling in an integrating sphere is simple and robust, so it has received a lot of attention because of its application in the compact cold atom clock [4–6].

The trapping of the Rayleigh dielectric sphere by partially coherent beam has been studied [7,8]. For the atomic cloud cooled by laser, it is found that its temperature depends on the intensity, detuning, and linewidth of the cooling laser [9–11]. However, the influence of the spatial coherence of the cooling lasers on the atoms has not been investigated before. It is interesting to explore the interaction between the partially spatially coherent laser and neutral atoms.

In this paper, the characteristics of the atoms cooled by lasers with various degrees of spatial coherence in a magneto-optical trap (MOT) are investigated both experimentally and theoretically. The spatial coherence of the cooling lasers is controlled by the electro-optic phase modulation of $LiNbO_3$ (LN) crystal [12,13]. We found that the temperature of the cold atomic cloud increases with decreasing degree of spatial coherence both in the MOT and polarization gradient cooling (PGC) experiments [14,15]. A theoretical analysis of the corresponding radiation force and motion of the atoms is also presented.

II. THE GENERATION OF A PARTIALLY SPATIALLY COHERENT LASER BEAM

The light propagates through the LN crystal along the z axis and a high ac voltage is applied on the crystal along the x axis, which can change the refractive index of the crystal. Therefore after the laser beam passes through the LN crystal, it can acquire an additional phase ϕ that is proportional to the external electric field intensity and is dependent on both the spatial position and time,

$$\phi \approx \frac{\pi}{\lambda} n_o^3 \gamma_{22} l \left\{ \sqrt{\left[\frac{\partial U(\mathbf{r},t)}{\partial x}\right]^2 + \left[\frac{\partial U(\mathbf{r},t)}{\partial y}\right]^2} \right\}, \quad (1)$$

where l is the length of the LN crystal, γ_{22} and n_o are the electro-optic coefficient and refractive index of the LN crystal respectively, λ is the wavelength of the laser beam, and $U(\mathbf{r},t) = U_0(x,y)\varphi(t)$ is the electric potential. Then the temporal and spatial terms of the additional phase can be separated as

$$\phi = \psi(x,y)\varphi(t). \quad (2)$$

Here the temporal term $\varphi(t)$ can be directly derived from the temporal term of the electric potential, and the spatial term $\psi(x,y)$ is deduced from the spatial distribution of electric potential in the transverse plane.

We simulated the instantaneous spatial distribution of the additional phase of the laser beam in the output plane of the LN crystal, and found it is not uniform (Fig. 1). In our simulation, the size of the LN crystal is $10 \times 10 \times 80$ mm; two electrodes (5×80 mm) are attached to opposite surfaces of the crystal.

After passing through the LN crystal, the electromagnetic field of the laser beam can be expressed as

$$\mathbf{E}(\mathbf{r},\mathrm{t}) = \mathbf{E}(\mathbf{r})\cos(\omega t - \mathbf{k}\cdot\mathbf{r} + \phi), \quad (3)$$

where ω is the angular frequency of the laser. The additional phase ϕ adds to the phase term of the laser. The degree of spatial coherence between two different positions $\mathbf{r}_1$ and $\mathbf{r}_2$ is

$$\gamma(\mathbf{r}_1,\mathbf{r}_2,0) = \frac{\langle \mathbf{E}(\mathbf{r}_1,t)\mathbf{E}^*(\mathbf{r}_2,t)\rangle_t}{\mathbf{E}(\mathbf{r}_1)\mathbf{E}(\mathbf{r}_2)}, \quad (4)$$

where the angular bracket $\langle\rangle_t$ denotes the time average. $\mathbf{E}(\mathbf{r}_1,t)$ and $\mathbf{E}(\mathbf{r}_2,t)$ are the fields at the two positions $\mathbf{r}_1$ and $\mathbf{r}_2$, respectively. The spatial coherence of the laser can be analyzed by inserting Eq. (3) into Eq. (4). The inhomogeneous spatial distribution and temporal oscillation of the additional phase degrade the spatial coherence of the laser beam. When the voltage applied on the LN crystal is higher, the spatial distribution of the additional phase is more inhomogeneous, which induces greater degradation of the spatial coherence of the laser beam.

*zhaoyingwang@zju.edu.cn
†qlin@zju.edu.cn

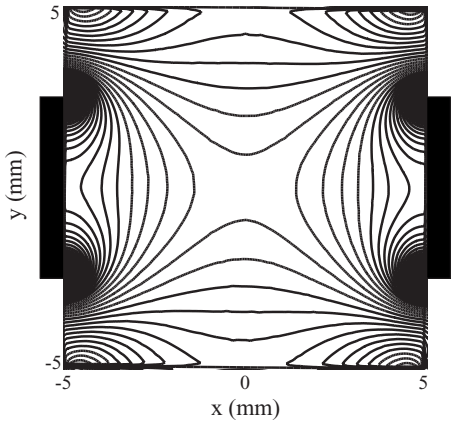

FIG. 1. The simulated instantaneous spatial distribution of the additional phase of the laser beam in the output transverse plane of the LN crystal. The two black blocks attached to the crystal represent the electrodes. The solid lines represent the equal magnitude contours of the additional phase.

Young's double pinhole experiment is employed to quantify the degree of spatial coherence of the modulated laser beam [16–18]. After passing through the LN crystal, the laser beam is expanded, and propagates through a double pinhole (Fig. 3). The intensity interference pattern measured in the charge coupled device (CCD) camera plane is

$$I\left(\mathbf{r}'\right) = I_1\left(\mathbf{r}'\right) + I_2\left(\mathbf{r}'\right) + 2\sqrt{I_1\left(\mathbf{r}'\right) I_2\left(\mathbf{r}'\right)}\,|\gamma| \times \cos\left(\frac{2\pi \mathbf{r}' \cdot d}{\lambda D} + C\right), \tag{5}$$

where $I_{1,2}(\mathbf{r}')$ are the intensities of the two fields out from the double pinhole in the observation plane, d is the pinhole separation, D is the distance from the double pinhole to the CCD, and C represents the slowly varying phase of the complex degree of spatial coherence. When the light intensities passing through the two pinholes are equal, the visibility of interference fringes is a good evaluation of the degree of spatial coherence of the modulated laser beam.

Double pinhole experiments with varying pinhole separations have been used to measure the degree of spatial coherence at different relative distances. The beam diameter of the laser is 15 mm. The double pinhole separation has been varied from 5 to 13 mm in the horizontal direction. When there is no phase modulation applied on the laser beam, the degree of spatial coherence decreases just a little when the pinhole separation is changed from 5 to 13 mm. When the double pinhole separation is 5 mm, the degree of spatial coherence is 0.97 ± 0.01. When the pinhole separation is 13 mm, the corresponding degree of spatial coherence is 0.91 ± 0.01, as shown by the closed circles in Fig. 2(a). While for the laser beam with phase modulation (the frequency and voltage of the applied ac electric field are set as 20 kHz and 3.4 kV, respectively), the change of the degree of spatial coherence is larger for different pinhole separations. When the pinhole separation is 5 mm, the degree of spatial coherence is 0.93 ± 0.01. When the pinhole separation is 13 mm, the corresponding degree of spatial coherence is 0.48 ± 0.01, as shown by the open squares in Fig. 2(a). We simulate the modulated laser beam using the Gaussian-Schell model [19]. The experimental result

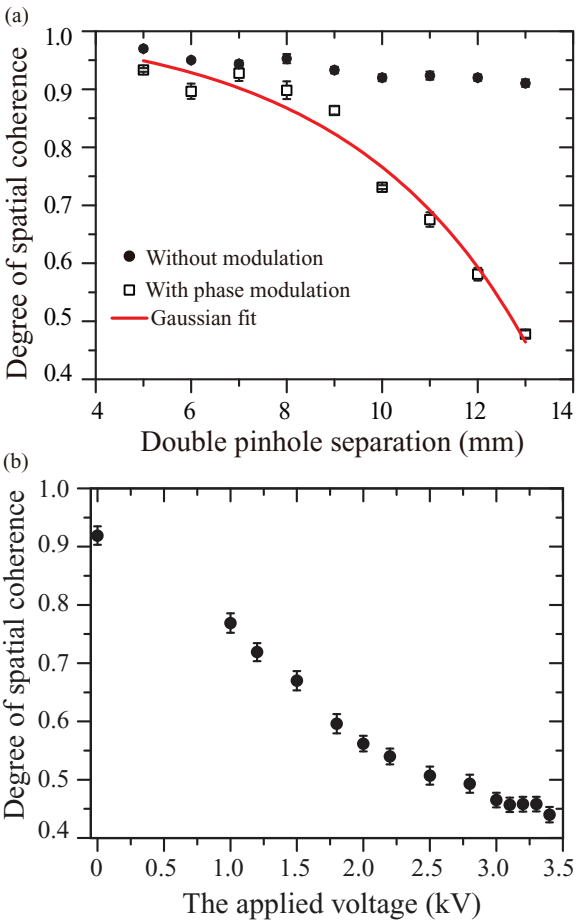

FIG. 2. (Color online) The degree of spatial coherence of the laser beam measured in the double pinhole experiments. The beam diameter of the laser is 15 mm. (a) The degree of spatial coherence varies with the double pinhole separation for laser without phase modulation (closed circles), and the laser with phase modulation; the corresponding frequency and voltage of the applied ac electric field are set as 20 kHz and 3.4 kV, respectively (open squares). The solid line represents the Gaussian fit of the experimental result of the laser with phase modulation. (b) The degree of spatial coherence of the modulated laser decreases along with the increasing applied voltage. The frequency of the applied ac electric field is 25 kHz. The double pinhole separation is set as 12 mm.

of the laser with phase modulation was fitted with the Gaussian function $\gamma(d) = \exp[-d^2/(2\sigma_g^2)]$, shown as the solid line in Fig. 2(a). Therefore the degree of spatial coherence of the modulated laser has a Gaussian decay with the double pinhole separation. That means the spatial coherence of the laser beam is degraded by the phase modulation.

The degree of spatial coherence of the laser beam decreases along with the increasing phase modulation applied on the laser. The beam diameter of the laser is 15 mm, and the double pinhole separation is set as 12 mm. The laser degree of spatial coherence without modulation is 0.92 ± 0.02. When the modulation is applied (the frequency of the applied ac electric field remains the same at 25 kHz), the degree of spatial coherence of the modulated laser decreases with the increasing applied voltage, as shown in Fig. 2(b). If the voltage of the applied ac electric field is set as 3.4 kV, the laser degree

of spatial coherence is reduced to 0.44 ± 0.01. In our case, the maximum frequency and voltage are 25 kHz and 3.4 kV, respectively. When a higher phase modulation is applied on the laser beam, the corresponding degree of spatial coherence can be lower. It is shown that the phase modulation can effectively degrade the spatial coherence of the laser beam, and the spatial coherence of the laser beam can be controlled by changing the phase modulation.

The phase modulation has very weak influence on the linewidth of the laser, which was confirmed by the measurement of the beat note bandwidth between the modulated laser and another reference laser. The measured bandwidth of the beat note signal is both 4.39 MHz for the experiment without phase modulation, and with 25 kHz modulation at 3.4 kV amplitude.

III. ATOM COOLING BY PARTIALLY SPATIALLY COHERENT LASERS

A continuous wave extended-cavity diode laser was used as the light source of the cooling laser, and was twice the natural linewidth red detuned from the $5\,^2S_{1/2}$, $F = 2 \rightarrow 5\,^2P_{3/2}$, $F' = 3$ of ^{87}Rb D_2 transition by an acousto-optic modulator (AOM). Another diode laser was used as a repumping laser to prevent the atoms from leaking out of the cooling transition, which was in resonance with the $5\,^2S_{1/2}$, $F = 1 \rightarrow 5\,^2P_{3/2}$, $F' = 2$ transition. The repumping beam and the cooling beam were coupled into the same single-mode polarization-maintaining fiber.

Figure 3 shows the experimental scheme of the atom cooling by the partially spatially coherent lasers. After passing through the LN crystal, the generated partially spatially coherent laser beam was expanded to 15 mm, and split into six independent beams to shine on the rubidium atoms in the MOT. The MOT is the three-dimensional (3D) $\sigma^+ - \sigma^-$ configuration. The intensity of each cooling beam is

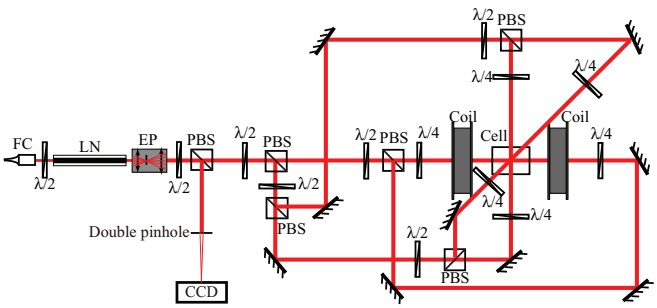

FIG. 3. (Color online) The schematic diagram of the atom cooling by partially spatially coherent lasers. The output beam from the fiber collimator (FC) passes though the LN crystal applied with a high ac electric field. Then the generated partially spatially coherent laser beam propagates through a beam expander (EP) before entering the MOT to cool the atoms. The half-wave plate ($\lambda/2$) and the polarization beam splitter (PBS) are used to split the light beams. After passing through the quarter-wave plate ($\lambda/4$), the counterpropagating beams are opposite ($\sigma^+ - \sigma^-$) circular polarized. A pair of anti-Helmholtz coils (Coil) is also used to provide the MOT magnetic field. A double pinhole and a charge coupled device (CCD) camera are used to measure the spatial coherence of the laser.

3.5 mW/cm^2, and the saturation intensity of ^{87}Rb atoms is 1.65 mW/cm^2. The magnetic field gradient at the center of the trapping zone is 10 G/cm.

We investigate the characteristics of the atoms cooled by the partially spatially coherent lasers both in the MOT and PGC experiments. In our experiment, the difference between the two is in the timing sequence. To perform the PGC, the magnetic field of the MOT is shut off; meanwhile we use the AOM to reduce the light intensity of the cooling laser to 10% of the initial intensity in 2 ms, and then preserve it for 5 ms before shutting off the laser completely. But we cannot ensure pure Doppler cooling in the MOT experiment, where the Doppler cooling is dominating and the influence of the PGC has been suppressed efficiently. That is because the PGC is very sensitive to the magnetic field [20,21].

Firstly, we investigate the atom number and density distribution of the atomic cloud cooled by the partially spatially coherent laser beams. A photodiode was used to monitor the laser induced fluorescence (LIF), whose intensity is proportional to the number of atoms in the trap. A CCD camera was located at one window of the MOT to image the atomic cloud.

In both the cooling experiments, the total atom number and atomic density distribution do not vary with the degree of spatial coherence of the cooling lasers. In every measurement, the total number of cold atoms remains the same at 2×10^8, and the spatial distribution of the atomic cloud remains Gaussian, either in the MOT or PGC experiment, as shown in Fig. 4. The Gaussian width is 1.73 ± 0.01 mm for the atoms cooled by the coherent beams, and is 1.78 ± 0.01 mm for the atoms cooled by the partially spatially coherent beams. The peak value of the atomic density is also the same.

Next, we investigate the temperature of the atomic cloud cooled by the laser beams with various degrees of spatial coherence in both the cooling experiments. The time-of-flight

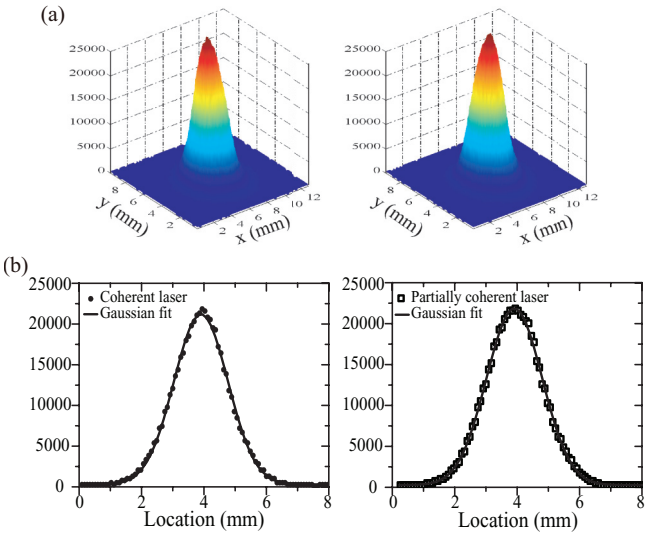

FIG. 4. (Color online) (a) Density distribution of the atomic cloud cooled by coherent lasers (left) and partially spatially coherent lasers (right) in the PGC experiment. (b) The cross sections of the atomic cloud for the spatially coherent laser cooling (left), and the partially spatially coherent laser cooling (right). The solid lines indicate the Gaussian fits to the measured atomic distributions.

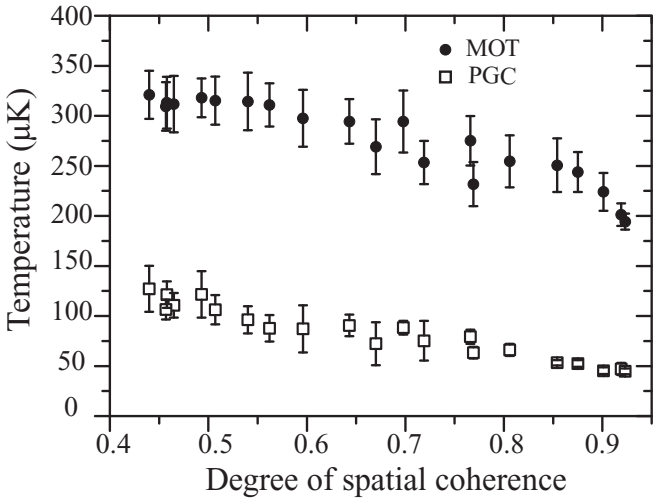

FIG. 5. The dependence of the temperature of the atomic cloud on the degree of spatial coherence of the laser beams in the MOT experiment (closed circles) and PGC experiment (open squares).

(TOF) technique was used to deduce the temperature of the cold atomic cloud [22–24]. The probe laser was resonant with the ^{87}Rb $5\,^2S_{1/2}$, $F = 2 \rightarrow 5\,^2P_{3/2}$, $F' = 3$ transition, and it was located 10 mm below the center of the atom trapping zone. After releasing the atomic cloud from the trap, the atoms fall due to gravity, and then pass through the probe beam. The light intensity of the probe laser is absorbed by the falling atomic cloud. The temperature of the atomic cloud can be obtained from the absorption signal curve.

In the MOT experiment, the temperature of the atomic cloud increases monotonously as the degree of spatial coherence of the laser beams decreases (closed circles in Fig. 5). When there is no phase modulation applied on the cooling lasers, the temperature of the atoms is 194 ± 8 μK. When the degree of spatial coherence is reduced to 0.44, the temperature of the atomic cloud increases to 321 ± 24 μK.

In the PGC experiment, the temperature of the cold atoms also varies with the various degrees of spatial coherence of the laser beams (open squares in Fig. 5). As the degree of spatial coherence decreases, the temperature of the cold atomic cloud also increases monotonously. When there is no modulation, the temperature of the atomic cloud is 45 ± 3 μK whereas when the degree of spatial coherence of the laser beams is reduced to 0.44, the temperature increases to 127 ± 23 μK.

IV. THEORETICAL EXPLANATION

The influence of the laser degree of spatial coherence on the atomic motion will be investigated theoretically. In the MOT experiment, the dipole force of the cooling laser is four orders of magnitude smaller than the scattering force, so the contribution of the former is negligible. The scattering force can be directly obtained from the steady-state solution of the optical Bloch equation [25,26] in the rotating wave approximation. Using the electromagnetic field assumption in Eq. (3), the scattering force is given by

$$F_z = \frac{\hbar\Gamma\Omega^2}{4(\Delta + kv + \partial_t\phi)^2 + \Gamma^2 + 2\Omega^2}k, \tag{6}$$

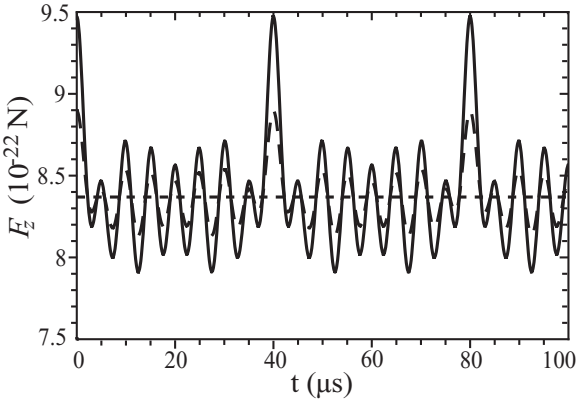

FIG. 6. The calculated temporal evolution of the scattering force F_z, assuming $\psi(x,y) = 0$ (short dashed line), $\psi(x,y) = \pi$ (long dashed line), and $\psi(x,y) = 2\pi$ (the solid line).

where Δ is the detuning of the laser from the atomic resonance, Γ is the atomic natural linewidth, v is the velocity of the atom, k is the wave number, and Ω is the Rabi frequency.

The term $\partial_t\phi$ in Eq. (6) corresponds to the additional phase that the partially spatially coherent laser obtained from the phase modulation. For the fully spatially coherent laser, the additional phase is equal to zero. Because the additional phase depends on the spatial position and time, it can cause the spatial and temporal fluctuations of the scattering force according to Eq. (6).

To illustrate the effect on the light pressure force of the reduced spatial coherence, the spatial and temporal variation of the force of a single beam caused by a fluctuating optical phase was analyzed theoretically. In addition, in the following Monte Carlo simulation of the atomic temperature, the laser is one dimensional, considering the cooling and heating effects of two counterpropagating beams. A full 3D model considering the effect of all six beams is beyond the scope of this paper.

Firstly, the temporal evolution of the scattering force F_z was calculated using Eq. (6) with assumption that $\psi(x,y)$ is constant (Fig. 6). For the fully spatially coherent laser [$\psi(x,y) = 0$], the scattering force is constant and does not vary with time. While for the partially spatially coherent laser, the scattering force oscillates with time. As $\psi(x,y)$ is larger, the amplitude of the temporal oscillation of the force is larger.

Meanwhile, according to Eq. (6), the scattering force also depends on the spatial position in the transverse plane. The instantaneous spatial distribution of the scattering force F_z of the partially spatially coherent laser is demonstrated in Fig. 7. As a result, the scattering force F_z of the partially spatially coherent laser has been proven to fluctuate strongly spatially and temporally.

The number of atoms in the MOT is determined by a balance between the capture rate into the trap and the loss rate from the trap [27–29]. The total atom number is

$$N = \frac{L^2}{\sigma}\left(\frac{v_c}{v_{th}}\right)^4, \tag{7}$$

where L is the laser beam diameter, σ is the cross section for collisions between the trapped atoms and the background vapor, $v_{th} = \sqrt{8k_BT/m\pi}$ is the average speed in the background vapor, T is the temperature of the background gas,

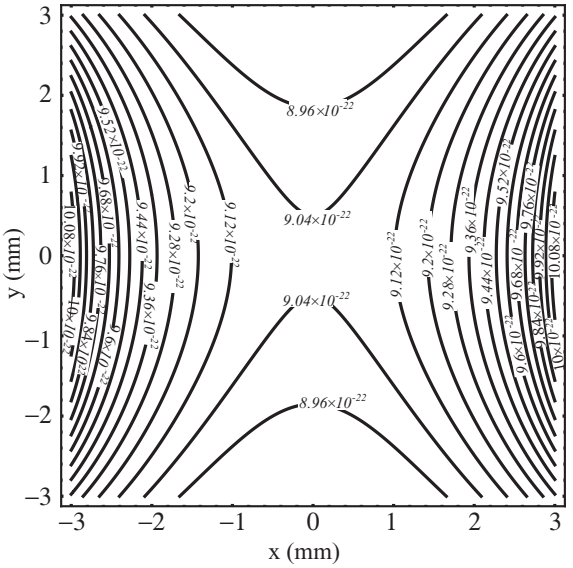

FIG. 7. The contour map of the instantaneous spatial distribution of the scattering force F_z of the partially spatially coherent laser. The solid lines represent equal magnitude contours of the scattering force. The contour spacing is 0.8×10^{-23} N.

and $v_c = \sqrt{2L\, v_{rc}\gamma_{sc}}$ is the maximum velocity of an atom that can be captured. $v_{rc} = \hbar k/m$ is the recoil velocity. The photon scattering rate γ_{sc} is given by

$$\gamma_{sc} = \frac{\Omega^2\Gamma}{\Gamma^2 + 4(\Delta + kv + \partial_t\phi)^2 + 2\Omega^2}, \tag{8}$$

which is proportional to the scattering force, and dependent on the term $\partial_t\phi$. But the average scattering rate does not vary with the phase modulation, which can be proven in Figs. 6 and 7. Then the capture velocity has an unnoticeable change for the partially spatially coherent laser. Therefore the spatial coherence of the cooling lasers has little influence on the total number of atoms. The long enough loading time can ensure a constant number of atoms, which is independent of the spatial coherence of the laser.

The atomic density is mainly limited by the photon scattering. As shown above, the average photon scattering rate does not vary with the spatial coherence of the cooling laser. Therefore the atomic density distribution changes little for the partially spatially coherent laser cooling.

In an attempt to study the influence of the fluctuating scattering force on the motion of atoms, a theoretical analysis by Monte Carlo simulation is carried out. We assumed that there are 10 000 noninteracting atoms with a Maxwell-Boltzmann velocity distribution. The spatial density distribution of the atoms is Gaussian. Considering the atom-laser interaction, the atoms can be damped by the scattering force, which results in a cooling effect. The momentum diffusion, which is due to the random nature of the absorption and spontaneous emission of the photons, causes the random walk in the atomic velocity space, and induces a stochastic heating of the atoms. After several tens of milliseconds, the cooling and heating effects produce a steady velocity distribution of the atoms, as shown in Fig. 8(a). After calculating the root-mean-square velocity of the atoms, the atomic temperature can be deduced.

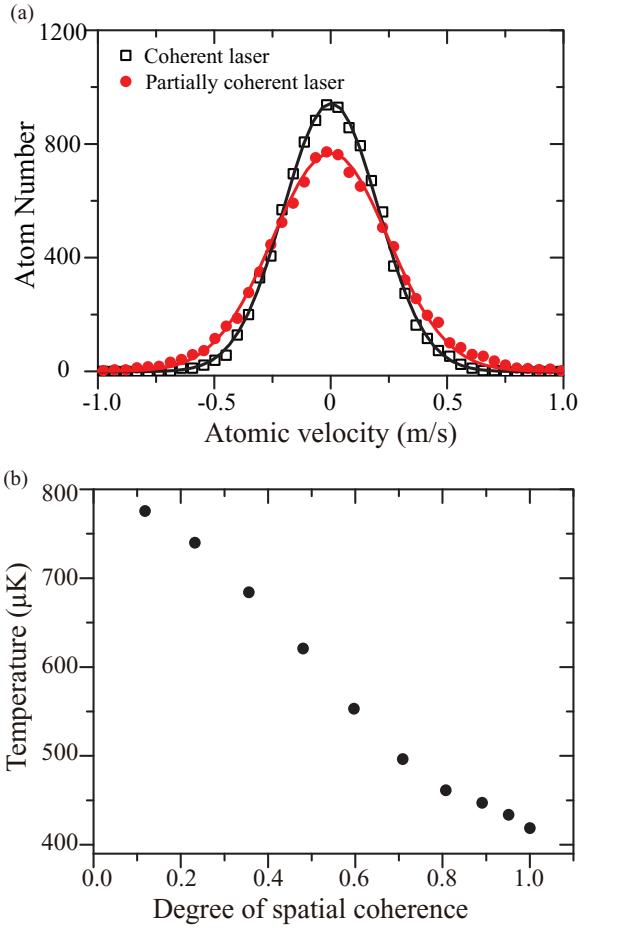

FIG. 8. (Color online) (a) The simulated atomic velocity distribution for the fully spatially coherent laser cooling (open squares) and the partially spatially coherent laser cooling (closed circles). The solid lines represent the Gaussian fits of the velocity distributions. (b) The calculated atomic temperature dependence on the degree of spatial coherence of the laser beams from the numerical simulation.

The calculated atomic temperature increases with the decreasing degree of spatial coherence of the cooling lasers in the Doppler cooling mechanism, as shown in Fig. 8(b). The theoretical simulation of the temperature change is the same as the experimental results shown in Fig. 5. For the partially spatially coherent laser cooling, the atoms at different spatial positions experience different scattering forces, which also fluctuate with time, and the temporal and spatial fluctuations of the force can produce an additional heating of the atoms. For the fully spatially coherent laser cooling, the scattering force acting on the atoms is independent of the position and time. As a result, the temperature of the atoms cooled by the partially spatially coherent lasers is higher than that by the coherent lasers.

The influence of the spatial coherence of the cooling lasers on the PGC temperature can also be analyzed. In the three-dimensional $\sigma^+ - \sigma^-$ configuration, the polarization of the fully spatially coherent laser beams is always linear, but rotates in space. For the partially spatially coherent laser, its additional phase varies with spatial position and time; as a result besides the temporal and spatial fluctuations of the force, the overall polarization of the laser beams is also disordered.

Therefore the phase modulation has a significant effect on the PGC. The temperature of the atoms can increase with the decreasing degree of spatial coherence of the cooling lasers. The theoretical calculation of the temperature of the atoms cooled by the partially spatially coherent lasers is very complicated in the PGC mechanism. Further research is needed to produce a rigorous treatment of temperature dependence on the degree of spatial coherence of the cooling lasers in the PGC mechanism.

V. CONCLUSIONS

In our experiment, the cooling laser can obtain an additional phase from the electro-optic modulation, which degrades the spatial coherence of the laser beam. We shined the partially spatially coherent lasers on the atoms in the MOT. The partially spatially coherent lasers can also cool and trap the atoms in the MOT. The total atom number and the atomic density distribution remain the same for the fully spatially coherent and partially spatially coherent beams. The main reason is that the average photon scattering rate is independent of the spatial coherence of the laser beams. While the temperature of the atoms cooled by the partially spatially coherent lasers increases as the degree of spatial coherence of the laser beams decreases. The reason for the increase of the temperature can be explained by the temporal and spatial fluctuations of the scattering force, which induce broader velocity distribution of the atoms. It is worth noticing that the effect of the spatial coherence of the cooling lasers on atoms also exists in the MOT configuration where the cooling beams are retroreflected, but the corresponding influence of the spatial coherence is smaller than that in the MOT setup with six independent laser beams.

ACKNOWLEDGMENTS

This work is supported by the National Natural Science Foundation of China under Grants No. 60925022 and No. 11174249, 973 Program (Grant No. 2013CB329501), the National High-Tech Research and Development Program of China under Grant No. 2011AA060504, and the Fundamental Research Funds for the Central Universities (2013FZA3002).

[1] H. D. Cheng, W. Z. Zhang, H. Y. Ma, L. Liu, and Y. Z. Wang, Phys. Rev. A **79**, 023407 (2009).
[2] W. Ketterle, A. Martin, M. A. Joffe, and D. E. Pritchard, Phys. Rev. Lett. **69**, 2483 (1992).
[3] E. Guillot, P. E. Pottie, and N. Dimarcq, Opt. Lett. **26**, 1639 (2001).
[4] F. X. Esnault, D. Holleville, N. Rossetto, S. Guerandel, and N. Dimarcq, Phys. Rev. A **82**, 033436 (2010).
[5] F. X. Esnault, N. Rossetto, D. Holleville, J. Delporte, and N. Dimarcq, Adv. Space Res. **47**, 854 (2011).
[6] X. C. Wang, H. D. Cheng, B. C. Zheng, Y. L. Meng, L. Xiao, L. Liu, and Y. Z. Wang, in *Proceedings of 2011 Joint Conference of the IEEE International Frequency Control Symposium and European Frequency and Time Forum* (IEEE, Piscataway, NJ, 2011), p. 1.
[7] C. L. Zhao and Y. J. Cai, Opt. Lett. **36**, 2251 (2011).
[8] C. L. Zhao, Y. J. Cai, X. H. Lu, and H. T. Eyyuboglu, Opt. Express **17**, 1753 (2009).
[9] A. Vorozcovs, M. Weel, S. Beattie, S. Cauchi, and A. Kumarakrishnan, J. Opt. Soc. Am. B **22**, 943 (2005).
[10] Y. Li, D. Yang, and Y. Wang, Acta Phys. Sin. (Overseas Ed.) **7**, 414 (1998).
[11] W. Z. Zhang, H. D. Cheng, L. Liu, and Y. Z. Wang, Phys. Rev. A **79**, 053804 (2009).
[12] Q. Lin and L. Wang, J. Mod. Opt. **50**, 743 (2003).
[13] P. Kolchin, C. Belthangady, S. W. Du, G. Y. Yin, and S. E. Harris, Phys. Rev. Lett. **101**, 103601 (2008).
[14] J. Dalibard and C. Cohen-Tannoudji, J. Opt. Soc. Am. B **6**, 2023 (1989).
[15] C. Salomon, J. Dalibard, W. D. Phillips, A. Clairon, and S. Guellati, Europhys. Lett. **12**, 683 (1990).
[16] R. A. Bartels, A. Paul, H. Green, H. C. Kapteyn, M. M. Murnane, S. Backus, I. P. Christov, Y. Liu, D. Attwood, and C. Jacobsen, Science **297**, 376 (2002).
[17] A. Singer, F. Sorgenfrei, A. P. Mancuso, N. Gerasimova, O. M. Yefanov, J. Gulden, T. Gorniak, T. Senkbeil, A. Sakdinawat, Y. Liu, D. Attwood, S. Dziarzhytski, D. D. Mai, R. Treusch, E. Weckert, T. Salditt, A. Rosenhahn, W. Wurth, and I. A. Vartanyants, Opt. Express **20**, 17480 (2012).
[18] H. Mashaal, A. Goldstein, D. Feuermann, and J. M. Gordon, Opt. Lett. **37**, 3516 (2012).
[19] S. R. Seshadri, J. Opt. Soc. Am. A **16**, 1373 (1999).
[20] M. Walhout, J. Dalibard, S. L. Rolston, and W. D. Phillips, J. Opt. Soc. Am. B **9**, 1997 (1992).
[21] M. Walhout, U. Sterr, and S. L. Rolston, Phys. Rev. A **54**, 2275 (1996).
[22] T. M. Brzozowski, M. Maczynska, M. Zawada, J. Zachorowski, and W. Gawlik, J. Opt. B **4**, 62 (2002).
[23] K. Pandey, K. D. Rathod, A. K. Singh, and V. Natarajan, Phys. Rev. A **82**, 043429 (2010).
[24] H. Hagman, P. Sjolund, S. J. H. Petra, M. Nylen, A. Kastberg, H. Ellmann, and J. Jersblad, J. Appl. Phys. **105**, 083109 (2009).
[25] R. J. Cook, Phys. Rev. A **20**, 224 (1979).
[26] P. J. Colmenares and J. L. Paz, Opt. Commun. **284**, 5171 (2011).
[27] M. Haw, N. Evetts, W. Gunton, J. V. Dongen, J. L. Booth, and K. W. Madison, J. Opt. Soc. Am. B **29**, 475 (2012).
[28] A. M. Steane, M. Chowdhury, and C. J. Foot, J. Opt. Soc. Am. B **9**, 2142 (1992).
[29] K. E. Gibble, S. Kasapi, and S. Chu, Opt. Lett. **17**, 526 (1992).